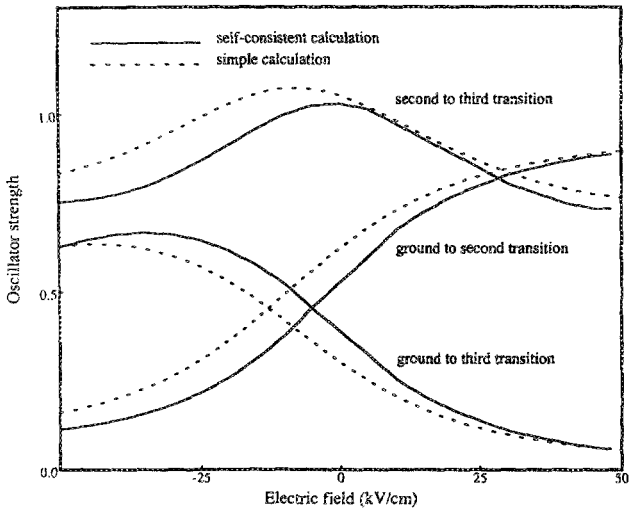

FIG. 3. Electric field dependence of the oscillator strength. The self-consistent result is similar to that of the simple calculation.

responds to a sheet charge density of $5.65 \times 10^{11}/\text{cm}^2$ and the Fermi level lies at 20 meV above the ground state, if deep traps are ignored and complete ionization of shallow donors is assumed. Since most of the carriers are distributed in the deep (right) side of the step well and the carriers come from the doped barriers, we found that about 70% of the carriers are from the right barrier and the remaining from the left barrier. Although the band bending is quite large in all three bias conditions, about 25 meV, the local and global energies seem to track closely, as in the case without band bending. At the same time, the wave functions retain their shapes even under various bias conditions.

In Fig. 2, we have calculated the transition energies as a function of the electric field for the same step well. It shows that in spite of the large band-bending effect, the self-consistent transition energies are quite close to those of simple calculation, with about 5 meV difference. (If the local exchange-correlation potential is ignored, the difference will be about 10 meV.) Thus, the large linear Stark shift of the LOG transition (the ground to second and ground to third in this case) is confirmed by this more accurate calculation. The oscillator strength versus field shown in Fig. 3 leads to the same conclusion. That is, the self-consistent analysis verifies that the oscillator strength is essentially the same as that of the simple calculation.

In summary, we have performed self-consistent calculations for the LOG transitions in a step well structure. Despite the fact that the band bending is large due to relatively high doping, the LOG transition is characterized by a large Stark shift and a large oscillator strength.

One of the authors (PFY) thanks Dr. D.S. Pan, Dr. J.M. Liu, Dr. S. Feng, and Dr. E. Carter for encouragement. This work is supported in part by the Office of Naval Research and Army Research Office.

[1]P. F. Yuh and K. L. Wang, J. Quantum Electron. **25**, 1671 (1989).
[2]P. F. Yuh and K. L. Wang, Phys. Rev. B **38**, 8377 (1988).
[3]Z. Ikonić, V. Milanović, and D. Tjapkin, J. Quantum Electron. **25**, 54 (1989).
[4]P. F. Yuh and K. L. Wang, J. Appl. Phys. **65**, 4377 (1989).

An experimental and theoretical investigation of electrostatically charged, falling droplet pairs

Scott A. Barton and Patrick F. Dunn
Department of Aerospace & Mechanical Engineering, University of Notre Dame, Notre Dame, Indiana 46556

(Received 1 November 1989; accepted for publication 20 December 1989)

Herein we report the results of an investigation of the trajectories of horizontally coplanar droplet pairs of similar charge, falling under the influence of gravity, drag, and electrostatic forces. Experiments were conducted using ethanol droplets that were generated electrostatically from the tips of two parallel needles. These droplets were subject to an external electric field and an initial electrostatic force in the vertical, downward direction, and an interdroplet electrostatic repulsive force in the horizontal direction. A model was developed to predict the measured trajectories. Within the range of applied potential differences investigated (from 1–3 kV), the theory and experiment were found to agree to within approximately 5%. The results also showed that the droplet trajectory was influenced noticeably by the axial electrostatic force on the droplet as it departed from the needle.

The production of micrometer-size liquid droplets by electrostatic means has been studied for well over two hundred years. Over the past twenty years, attention has focused on exploiting this process for practical use. Here, emphasis has been placed on relating the operating characteristics of various electrostatic droplet generators to their resultant droplet size, specific charge, and velocity. Numerous applications have developed, ranging from the everyday

 0021-8979/90/063201-04$03.00

applications of ink-jet printers,[1] paint and crop sprayers,[2] to those of colloid thrusters[3] and liquid droplet radiators[4] for use in space.

In some of these applications, multiple parallel streams of droplets must be produced from needle or micro-orifice arrays. Because the resultant droplets usually carry a similar charge, they are repelled from one another during transit. A primary concern then is to relate these droplet trajectories to the device's design, with the eventual goal of being able to predict droplet trajectories as a function of the device's operating conditions.

The present study deals with a very basic part of this problem, that is, to determine the trajectories of horizontally coplanar droplet pairs in air that emanate from two adjacent needles of an electrostatic droplet generator, as depicted in Fig. 1. These droplets are produced in a specific electrohydrodynamic operating regime of the generator, in which a relatively small applied potential (up to approximately 4 kV) exists between the generator and a distant, electrically grounded plate. In this regime, the droplets produced range in diameter from approximately 500 to 2000 μm and have specific charges from approximately 1×10^{-4} to 1×10^{-6} C/kg, respectively, as compared to the specific charges for droplets charged to their Rayleigh limit, which range from approximately 1×10^{-3} to 1×10^{-4}.

Our model of this process considers a force balance applied to a pair of inflight droplets of similar spherical diameter, d_d, mass, m_d, and charge, q_d. In this model, three key assumptions are made to match with those conditions of the subject experiments. First, the spacing between droplets emanating from an individual needle is assumed to be large enough so that electrostatic effects between such droplets are negligible. Second, each falling droplet is paired with another originating from the other needle and the resultant droplet pairs are horizontally coplanar. Third, the radial electric field between the needles and the ground plane is negligible in this region. Newton's second law, including gravitational, F_G, aerodynamic drag, F_D, and electrostatic, F_E, forces, for this system can be written as

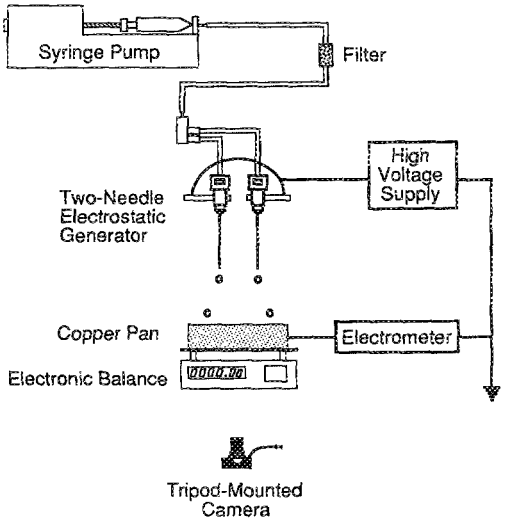

FIG. 1. Schematic of the experimental setup.

$$m_d \frac{d\bar{V}}{dt} = \bar{F}_G + \bar{F}_D + \bar{F}_E,$$

where

$$\bar{F}_G = m_d\, g\hat{\mathbf{z}},$$

$$\bar{F}_D = \frac{-C_D \pi \rho_m d_d^2}{8}\sqrt{V_r^2 + V_z^2}\,\bar{V},$$

$$\bar{F}_E = \frac{q_d^2}{4\pi\epsilon_0 S^2}\hat{\mathbf{r}} + q_d E_z \hat{\mathbf{z}},$$

and $\bar{V}$ denotes the droplet velocity, which equals $V_r\hat{\mathbf{r}} + V_z\hat{\mathbf{z}}$, C_D the drag coefficient, E the electric field strength, ρ_m the medium (air) density, g gravitational acceleration, S the distance between the droplets in a pair, ϵ_0 the permittivity of free space (8.85E-12 F/m), which closely approximates that in air, and r and z the radial (horizontal) and axial (vertical) coordinates, respectively.

This vector equation can be separated into its scalar components, which can be solved readily by standard Runge–Kutta numerical integration after reduction to the following system of four coupled equations:

$$\frac{dR}{dt} = V_r, \quad \frac{dZ}{dt} = V_z, \quad \frac{dV_r}{dt} = C - DV_r\sqrt{V_r^2 + V_z^2},$$

$$\frac{dV_z}{dt} = g - DV_z\sqrt{V_r^2 + V_z^2} + H_z,$$

where $R = S/2$, $C = q_d^2/16\pi\epsilon_0 m_d R^2$, $D = C_D\pi\rho_m d_d^2/(8m_d)$, $H_z = E_z q_d/m_d$ and with the boundary conditions $R(0) = S_0/2$, $Z(0) = 0$, $V_r(0) = 0$, and $V_z(0) = 2F_{E_z}(0)/\dot{m}$. The droplet drag coefficient, C_D, is a function of the Reynolds number, Re, which equals $\rho_m d_d\sqrt{V_r^2 + V_z^2}/\mu_m$. The expression used herein is $C_D = 24(1 + 0.15\,\mathrm{Re}^{0.687})/\mathrm{Re}$. This is that reported by Schiller and Naumann[5] for $1 \leqslant \mathrm{Re} < 800$, which is an empirical formula that most closely matches measured values for the Reynolds number range of the present experiment ($2 < \mathrm{Re} < 325$).

Because no accurate methods have yet been developed to predict size and specific charge of electrified droplets as a function of independent system parameters for this configuration, these quantities were specified *a priori* as inputs to the model. These inputs were the physical properties of the medium and working fluid (ρ_f, μ_m, ρ_m), the needle spacing (S_0, here 1.5 cm), the droplet specific charge (q/m), and the droplet diameter (d_d).

For the present analysis the coefficient H_z was determined by conservatively assuming a uniform electric field (a linearly varying electrostatic potential) in the axial direction equal to the potential difference between the needles' tips and the collection pan divided by that distance. The downward, vertical electrostatic force on the droplets immediately prior to their departure from the needles' tips, $F_{E_z}(0)$, is given by Bailey[2] for a charged pendant drop at the tip of a needle located above a grounded plane:

$$F_{E_z}(0) = \frac{\phi^2}{4\ln(2L/r_n)} + \phi^2 \int_0^L \left(\frac{1}{\ln\{[4x(2s_{np}+x)]/r_d^2\}}\right)^2 \times \left(\frac{dx}{(2s_{np}+x)}\right),$$

where ϕ denotes the potential difference between the needles' tips and the collection pan, s_{np} that distance (383 cm), L the needle length (1.905 cm), r_n the needle outer radius (203 μm), r_d the droplet radius, and x the distance measured in the upward direction along the needle's axis from the bottom of the droplet. Bailey's expression, which is valid when $L \gg 2r_n$, was developed from that presented by Van Dyke[6] for a semi-infinite cylinder. For simplicity, in the above expression, it is assumed that the droplet is spherical as it leaves the needle, which yields the r_d^2 term under the integral.

The experimental apparati, as shown in Fig. 1, basically consisted of a fluid delivery system, and two-needle electrostatic droplet generator, a droplet collection system, and associated diagnostic instrumentation. The reader is referred to Snarski[7] for details on the design and specific dimensions of the system, and to Barton[8] for details of the procedure for these experiments.

Liquid ethanol was supplied to the droplet generator at approximately 1.5 mℓ/min. A copper pan, was connected electrically through an electrometer to ground to monitor the droplet current. An electronic balance measured temporally the accumulated mass of the liquid. Photographs of the falling droplets were taken using a 35-mm camera. The average specific charge, q/m, was determined by the ratio $I/\dot{m}$, where I and $\dot{m}$ were averages determined by linear regression fits to the data.

A Cline–McClintock[9] error analysis was conducted to determine the standard uncertainty in the droplet positions for both the experimentally and analytically determined values. The results yielded standard uncertainties of 5.2% and 0.41% for the experimentally determined radial and axial positions, and 6.6% and 0.03% for the analytically determined radial and axial positions. The most significant uncertainty was in the needle spacing, which was 3.3%.

The analytically and experimentally determined droplet trajectories are shown for comparison in Fig. 2. For each applied voltage case investigated, the error associated with the analytical results is defined in the figure by dashed lines about those results. The error associated with the experimental data is presented with error bars. There is, in general, very good agreement between the measured and predicted values. The maximum percentage difference between them is 7.5%, which occurred for the 2 kV case at the greatest axial distance examined. This, however, is still within the combined analytical and experimental error in the radial position, which is 12%. All other data agreed with the theory to within the 5.2% experimental error in the radial direction.

Also apparent from the figure is the increasing droplet trajectory divergence that occurs in the radial direction with increasing applied voltage. This anticipated trend results

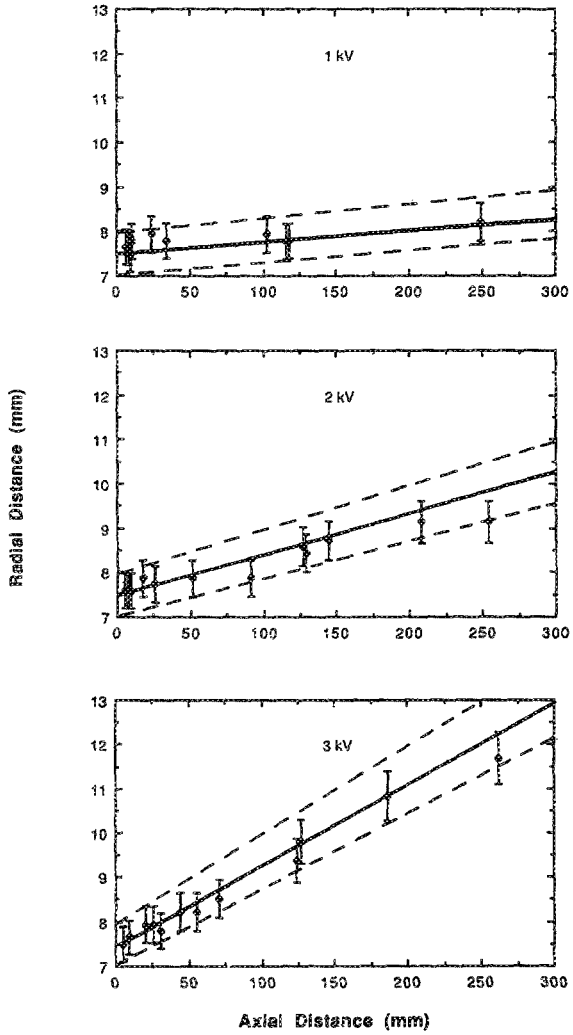

FIG. 2. Comparison of experimental and theoretical results.

from the increased droplet specific charge that occurs with increasing applied voltage (from approximately 1E-5 C/kg at 1 kV to 5E-5 C/kg at 3 kV). Further, the data acquired at large axial distances for the 2 and 3 kV cases are somewhat overpredicted by the theory (by approximately 5 to 7%). This probably is the result of underestimating either the axial electric field strength or the initial droplet velocity in the axial direction. An increase in the magnitude of either one would limit further trajectory divergence because of the resulting increase in droplet acceleration in the axial direction.

The sensitivity of the analytical results to these two assumptions can be examined further. The effect that an external axial electric field has on the droplet trajectories can be ascertained by performing additional calculations in which this field, E_z, is neglected. These results are compared with those obtained from the model presented beforehand which includes the axial field. Both analytical results and the experimental results are shown in Fig. 3 for the 3 kV case, which was chosen because the greatest comparative differences occur for this case. The solid line in the figure denotes the analytical predictions including the field and the dashed line the predictions without it. The greatest difference between the two analytical cases is less than 1%. These re-

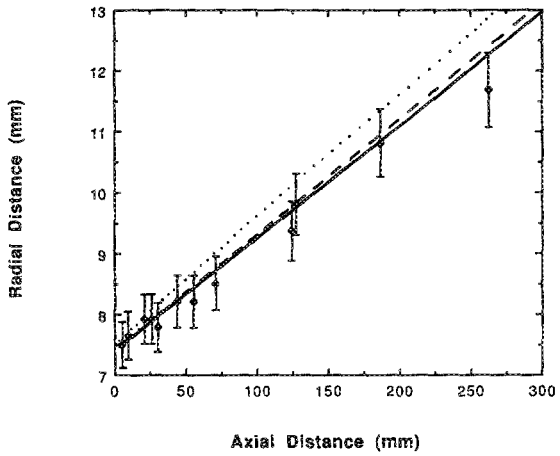

FIG. 3. Comparison of underlying theoretical assumptions for the 3-kV case.

sults support that the axial electric field has little influence on the droplet trajectories for the conditions examined.

Likewise, the effect of the axial electrostatic force on the droplet at the instant of separation from the needle, $F_{E_z}(0)$, can be determined. The dotted line in Fig. 3 represents the analytical case in which both the axial electrostatic force, $F_{E_z}(0)$, and the axial electric field, E_z, are neglected. The greatest difference between this case and that obtained from the model assuming an axial electric field and an initial electrostatic force is approximately 9%. These computational results suggest for experiments in which droplets are generated with moderate specific charges above a distant grounded plate, that, in addition to the normal electrostatic repulsive and drag forces, the droplet trajectories can be noticeably influenced by an initial electrostatic force that results in an initial droplet axial velocity. Further, from these results, it seems likely that the aforementioned overprediction of the droplet radial position at large axial positions is probably the result of a slight underprediction of the droplet's initial axial velocity.

In summary, we have found that the measured droplet trajectories for such electrostatic droplet generators operated under the subject conditions can be predicted to within approximately 5% and that the axial electrostatic force acting on the droplet as it departs from the needle's tip can significantly influence its trajectory.

The present work was conducted as part of ongoing research efforts to elucidate the droplet characteristics of electrohydrodynamic sprays. A majority of this work constitutes a research study conducted by S. Barton that was presented at the 1989 Region III AIAA Student Paper Conference in Cincinnati, OH. Partial support from the University of Notre Dame and from the AIAA Region III St. Joseph Valley Section is acknowledged.

[1]IBM J. Res. Dev. **21**, No. 1 (1977).
[2]A. G. Bailey, *Electrostatic Spraying of Liquids* (Wiley, New York, 1988).
[3]A. G. Bailey, J. Phys. D **6**, 276 (1973).
[4]A. T. Mattick and A. Hertzberg, J. Energy **5**, 387 (1981).
[5]R. Clift, J. R. Grace, and M. E. Weber, *Bubbles, Drops and Particles* (Academic, New York, 1978), p. 111.
[6]M. D. Van Dyke, Proc. R. Soc. London Ser. A **313**, 471 (1969).
[7]S. R. Snarski, M. S. thesis, University of Notre Dame, 1988.
[8]S. A. Barton, Particle Dynamics Laboratory Report No. UND/AME/PDL/SAB-89-1, University of Notre Dame, 1989.
[9]S. J. Kline and F. A. McClintock, Mech. Eng. **75**, 3 (1953).

On a resonant-mass superconducting antenna coupled to a resonant inductance transducer

Huei Peng
Physics Department, The University of Alabama in Huntsville, Huntsville, Alabama 35899

(Received 20 March 1989; accepted for publication 20 December 1989)

We show that the gravitational-wave-induced electric field in a superconducting antenna coupled to a reconant inductance transducer is much smaller than that in a superconducting antenna without a transducer. The superconductivity property of a superconducting antenna produces an addtional shift in the resonant frequency of the displacements which might be detectable, although it is small.

As is well known,[1] the predicted effects of general relativity regarding moving sources, i.e., gravitomagnetic effects and gravitational waves (GW), have yet to be directly tested. In order to reduce the thermal noise, it has been expected to operate the GW bar detectors with as low an antenna temperature (T_a) as possible.[2,3] One of the major features of plans for the third generation of resonant-mass antennas is the use of an ultralow temperature of 10–50 mK.[4] At this T_a, an aluminium bar becomes a superconductor. Hereafter we will refer to antennas with the temperature lower and higher than the critical temperature T_c as the S and N antennas, respectively. When one deals with an S antenna it is neces-

 0021-8979/90/063204-04$03.00